Rib channel chirowaveguides: A simple way to free the integrated photonics from linear polarizations monopoly

Hoshang Sahib, Alban Gassenq, Amina Bensalah-Ledoux, Bruno Baguenard, Laure Guy, Stephan Guy

Rib channel chirowaveguides: A simple way to free the integrated photonics from linear polarizations monopoly

*H. Sahib A. Gassenq A. Bensalah-Ledoux B. Baguenard L. Guy S. Guy **

H. Sahib, A. Gassenq, A. Bensalah-Ledoux, B. Baguenard, S. Guy
Univ. Lyon, Institut Lumière Matière, UMR 5306 CNRS-Université Claude Bernard Lyon 1, 10 rue Ada Byron, 69622 Villeurbanne Cedex, France
Email Address: stephan.guy@univ-lyon1.fr
L. Guy
Univ. Lyon, ENS de Lyon, CNRS Laboratoire de Chimie UMR 5182, Université Claude Bernard Lyon 1, F-69342, Lyon, France

Keywords: *Photonics, Polarization, Chirality, Chirowaveguides*

One fundamental law in integrated photonics (IP) is the decomposition of the guided optical waves into two independent linearly transverse polarization modes: the TE and TM modes. Because of the planar symmetry of on chip devices that induces linear birefringence (LB) in these systems, the use of IP is limited to the area where the relevant polarization modes are the linear ones. Using hybrid organic-inorganic chiral material with high circular biregringence (CB), we susscefuly achived channel sol-gel chirowaveguides via a simple imprint technique. By varying the channel chirowaveguides geometry and consequently, balancing LB and CB, elliptical birefringence could be tuned and eigenmode polarization from linear to nearly circular could be propagated in these unique waveguides. Our study unravels a new way of polarization control in IP, providing a route towards the design of versatile optical chirowaveguides in which light can propagate through eigenmodes with a polarization other than linear.

Symmetry basics are behind the polarization properties of light through its interaction with matter.[1, 2, 3] In an isotropic material, all polarization states of the light can propagate without being modified : they are all eigenmodes. When a medium, or a device, departs from a homogeneous state possessing all spatial and temporal symmetries, only two polarized waves can propagate without modification: they are the eigenmodes, orthogonal to each other with different phase velocities.[1, 2]
Integrated photonic (IP) merges the advantages of optics and integrated circuits in a single chip that can have many applications like sensing or communication. IP circuits are basically fabricated on planar substrates (often called chips). Furthermore, components used in IP are made of 2D structured planar waveguides with rectangular like cross-sectional shape. These 2D structured planar waveguides with their ability to confine light in the two transverse directions are essential to provide the connections between optical components and are called channel waveguides. They are building blocks of many IP components such as waveguide couplers, Mach-Zehnder interferometers, arrayed-waveguide gratings or ring resonators.
The loss of the translational symmetry in one direction, orthogonal to the chips plan, for planar waveguides and in two directions for channel waveguides induces a shape-anisotropie and thus a linear birefringence (LB) in these systems. Indeed, The TE and TM polarization eigen modes propagate with different phase velocities which results in different effective refractive indices for these two eigen modes. Any other polarization state of the light, other than TE and TM, which passes through these asymmetric systems in guided mode, will necessarily decompose between the two eigen modes. Consequently, it is difficult if not impossible to propagate eigen modes with other polarization than transverse linear in IP standard components (Figure 1-a). Thus, all the areas where the key polarizations are not linear cannot afford the advantages of IP: robustness, integration, mechanical insensitivity, low price among others. [4, 5]
The main idea of this work is the use of chiral materials to allow the propagation of eigen modes with polarization other than linear in IP components, (on peut rajouter si vous voulez: overcoming thus, the TE/TM polarization modes limitation) . Indeed, the odd parity inversion symmetry makes isotropic chiral media circular birefringent[6]: right/left-handed circularly polarized(R/LCP) waves are then the two eigenmodes (Figure 1-c,d) and the circular birefringence (CB) is defined as difference between the effective refractive indices of the RCP and LCP. Here, the mode beating (mixing between the two circular polarizations propagating through the chiral medium) results in the well known optical rotation, i.e.

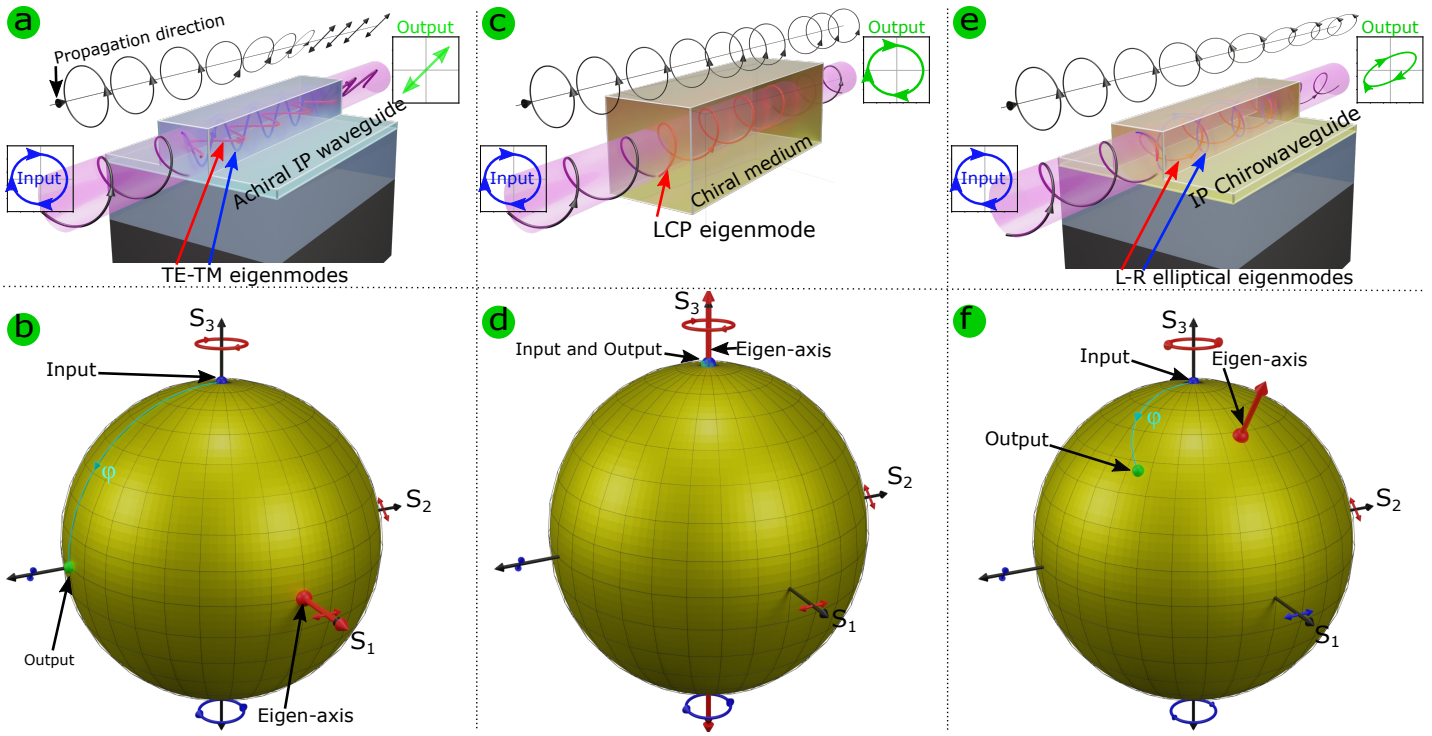

Figure 1: Concept of polarized wave transformation in birefringent systems in real space (a,c, and e) and Poincaré sphere (b,d,and f). An input polarized wave propagating through these systems decomposes into two orthogonal polarized waves called eigenmodes. In Poincaré sphere (PS), the two eigenmodes create a diameter axis (eigen-axis) in which the birefringence effect on any input wave other than the eigenmodes is a rotation of the input around the eigen-axis. The value of rotation angle (φ) depends on interaction length (l) and the difference of effective refractive indices of the two eigenmodes (Δn). In Poincaré sphere, φ give by eq.5, here, $(l\mathrm{MB}/\lambda) = \lambda/4$ then $\varphi = 2\pi$ in which the achiral waveguide behaves as a quarter waveplate. **a-b)** IP waveguides made of standard (achiral) materials are linear birefringence systems. TE/TM are their two eigenmodes ($\pm S_1$). **c-d)** Chiral media are circular birefringence systems. R/L CP are their two eigenmodes($\pm S_3$). Combination of linear (IP) and chiral birefringence results into **e-f)** IP chirowaveguides which are elliptical birefringence systems. Their eigenmodes are between TE/TM and R/L-CP which is defined by eq. 4.

the rotation of the polarization's state orientation proportional to the sample path. As already pointed out by Poincaré in 1892 [7], combination of linear and circular birefringences leads to the elliptical birefringence where the eigenmodes are in between TE/TM and R/LCP. Thus, IP devices made from chiral materials should be, by nature, elliptical birefringent (Figure 1-e,f). Furthermore, as shown on the same Figure, conservation of propagated circularly polarized waves is much more effective in chiral media and chirowaveguides compared to achiral waveguides. (ce n'est pas assez bien expliqué pourquoi comment , ...etc

Chiral optical waveguides have already been deeply studied starting from Engheta and Pellet who firstly named "chirowaveguides" the optical waveguides made of a chiral core [8, 9, 10, 11]. However, practical realization of such waveguides is rare as LB has much higher values than CB and therefore, prevents the effect of the latter. Indeed, in the multipolar description of the light material interaction, chirality appears as a second order effect and is thus much lower than the linear one. The ratio between linear and chiral effects is given by L/λ where L is the typical length of the molecules and λ is the vacuum wavelength. For a standard chiral molecule size ($L \leq 1nm$) in the visible range ($\lambda \sim 500nm$), chiral effect is then three orders of magnitude smaller than the linear effect. Noteworthy, the highest CB (1×10^{-3}) are measured in crystals while the highest CB values for amorphous polymers doped with chiral molecules are around 1×10^{-5} [12, 13, 14]. To compare, LB coming from residual molecular orientation in disordered polymers is in the order of 1×10^{-3} [15]. Thus, without reducing the LB, it is difficult to evidence the chirality effect in chirowaveguides and to propagate non linear polarization eigenmodes in elliptical birefringent devices for integrated photonics.

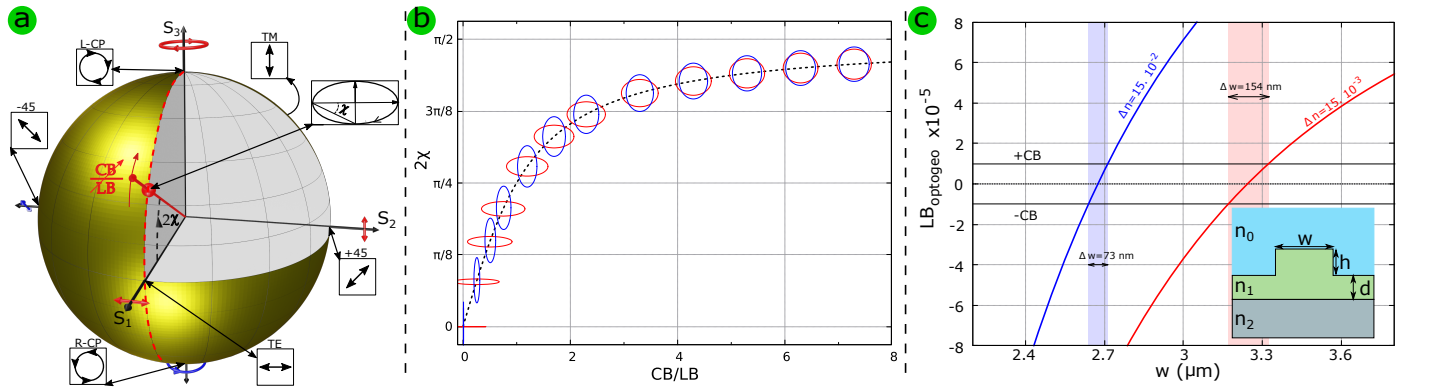

Figure 2: **a)** Poincaré sphere representation: The eigenmodes of a chirowaveguide are on the meridian, drawn in red dotted lines, containing the linear and circular birefringence. By varying the CB/LB ratio, The polarization ellipticity angle (2χ) can be tuned from 0 (TE mode) to $\pi/2$ (circularly polarized mode). **b)** Plot of 2χ with the corresponding polarization ellipses as a function of CB/LB. **c)** Computed $LB_{optogeo}$ (n_{TE00}-n_{TM00}) for a rib waveguide (inset) with d = 0.2 µm, h=2.1 µm and n_2=1.61 for two refractive index contrasts ($\Delta n = n_1 - n_2$)

In optical waveguides, two main effects give rise to LB: (i) the optogeometrical effect related to the refractive index contrast between the guiding layer and the surrounding and to the shape and dimensions of the waveguide ($LB_{optogeo}$) and (iii) the residual stress effect related to photoelasticity (why photoelasticity, do you mean the elasticity of the material?) (LB_{stress})[16]. Several solutions have been proposed to reduce the LB such as design of zero birefringence waveguides [17, 18, 19, 20, 21] or control of the LB intrinsic to the waveguides by creating external LB_{stress}[22, 23]. In all these examples, the fabrication constraints are tedious if achiral material is used since it is necessary to control waveguide dimensions with nanometer precision throughout the propagation length. Hopefully, the use of chiral materials relieves the fabrication constrains depending on the value of CB as shown in Figure 2-c. Planar Waveguides made of chiral materials with high CB and controlled $LB_{optogeo}$ in thick symmetrical structure are used to realize planar chirowaveguides with elliptical birefringence related properties.[13, 14] However, for practical applications, these planar chirowaveguides can only confine light in one dimension while two-dimensional light confinement is necessary for IP components.
Here, we report on the fabrication of elliptical birefringent rib waveguides in order to develop and achieve elliptical birefringent IP components. Both the material (a chiral hybrid silica material with CB=10^{-5}) and microstructures are realized via two simple, low cost, and low temperature methods which are sol-gel and imprint lithography respectively. For the given CB value, the LB value of the fabricated rib waveguides have been tailored by varying the channels width on the same sample [18, 24]. In doing so, we straightforward optimized the geometry of the channel chirowaveguide and obtained polarization eigenmodes with ellipticity[1] as high as $\pi/5$.
Our work shows that, thanks to the use of chiral materials, any polarization of light , from linear to circular, can be an eigen mode that propagates without modification in geometrically well adapted integrated photonic circuits and that TE and TM are not any more the unique relevant eigen modes for IP. This achievement can also open exciting perspectives in all areas where polarization modes other than TE/TM are the key tools such as for biological imaging[25], chiral sensing[26] or quantum information[27].

1 Model and structure design

Model: The combination of chirality through CB and LB of chirowaguides can be modeled using the coupling mode theory[12, 28, 29]. For a waveguide with given optical and geometrical properties, the unperturbed system corresponds to the achiral one with linear birefringence and TE/TM eigenmodes. If we

[1] ellipticity is shape parameter which is defined as the degree to which an ellipse is circle, it can take values between $-\pi/4$ and $+\pi/4$

consider here, a waveguides that support only two fundamental polarization modes (TE_{00} and TM_{00}), we can write according to The theory given in references [12, 28, 29], the coupling hamiltonian H_0 as follow:

$$H_0 = \frac{-ik_0}{2}\begin{bmatrix} \mathrm{LB} & i\mathrm{CB} \\ -i\mathrm{CB} & -\mathrm{LB} \end{bmatrix} \tag{1}$$

where k_0 is the vacuum wavevector. The H_0 diagonal terms describe the unperturbed achiral system characterized by its LB while the off-diagonal terms couple the unperturbed TE and TM modes. The coupling hamiltonian shows in a compact form that the whole system is completely described by only the two birefringences LB and CB. Diagonalizing H_0 reveals two elliptically polarized eigenmodes of modal birefringence (MB)[12, 28, 29]. The Jones vectors of the eigenmodes and MB are given by :

$$|+>= \begin{bmatrix} \cos\chi \\ -i\sin\chi \end{bmatrix}, \qquad |->= \begin{bmatrix} \sin\chi \\ i\cos\chi \end{bmatrix}, \tag{2}$$

$$\mathrm{MB} = \sqrt{LB^2 + CB^2} \tag{3}$$

where the ellipticity χ is defined as

$$\tan 2\chi = \frac{\mathrm{CB}}{\mathrm{LB}} \tag{4}$$

On the Poincaré sphere (PS), these two eigenmodes are represented by the two extremities of the diameter axis (eigen-axis) of latitude 2χ in the plane defined by the axes of linear ($\pm S_1$) and circular ($\pm S_3$) birefringence. They are thus, located on the meridian of longitude $2\psi = 0$ (dashed red curve in Figure 2-a). To remind, PS is a representation of polarization states of light very well adapted to the birefringent systems description [30, 31]. All the polarizations states are mapped on the sphere where the properties of a polarization ellipse such as ellipticity, orientation, and handedness of the polarization are coded via half the latitude angle χ, half the longitude angle ψ and north vs south hemisphere, respectively (Figure 2-a). A birefringent device changes any input polarization state into an output polarization state by rotating the input around its eigen-axis. The value of the polarization rotation φ is proportional to MB and the birefringent device's length (l):

$$\varphi = k_0 \cdot \mathrm{MB} \cdot l = \frac{2\pi}{\lambda} \cdot \mathrm{MB} \cdot l \tag{5}$$

From Eq. 2-4, chirowaveguides are elliptical birefringent devices with (i) main axis identical to the linear birefringent unperturbed system, (ii) ellipticity related to the CB/LB ratio via Eq.4 and (iii) birefringence given as the arythmetic average of the circular and linear birefringences (Eq.3). The effect of a chirowaveguide on an input polarization is represented on the PS (Figure 1-f) as a rotation φ around the eigen-axis of latitude 2χ and longitude given by the linear birefringence axis (0 for TE/TM axis). The sign of χ defines the polarization handedness, the 2χ is measured as the angle between the equatorial plane, and the slow eigenmode (the one with the higher effective refractive index). For instance, the slow eigenmode being in the south, it corresponds to a negative χ and thus, left-handed polarization state. By modulating CB/LB from 0 to ∞ : all the ellipticities can be accessed as it is illustrated by Figure 2-b. As expected, for CB=0 ($2\chi = 0$), the device is purely linear birefringent and corresponds to the the standard achiral optical waveguide with TE/TM eigenmodes (Figure 1-a,b). When LB=0 ($2\chi = \pi/2$) the waveguide behaves as an isotropic circular birefringent waveguide with R/LCP eigenmodes (Figure 1-c,d). Intermediate values of χ correspond to elliptical birefringent devices (Figure 1-e,f). From the design point of view, our objective is to make a waveguide with dominant chirality ($|\mathrm{LB}| \leq |\mathrm{CB}|$). In term of ellipticity angle, from Eq. 4, it corresponds to $\chi > \pi/8$.

Design: As discussed above, the ellipticity of the eigen polarization is ruled by the ratio CB/LB. Our goal involves to maximize CB and minimize LB, simultaneously in order to access the highest eleptical birefringence possible. Optimization of the CB value has been reached by the achivement of multilayers based chirowaveguides made from an optically active chiral sol-gel polymer developed previously in our

group [32]. The material is basically an organically modified silica (ORMOSIL) that allowed reaching CB = 1 x 10^{-5}, among the highest described for amorphous polymer materials.
Regarding the LB minimization, we have combined two strategies to obtain the lowest LB possible. As mentioned before, total linear birefringence of the guiding layer LB has several contributions: $LB_{optogeo}$ resulting from its refractive index contrast and geometry and LB_{stress}, the residual stress birefringence contribution arising from different sources of stress[22]. Our first strategy was to reduce $LB_{optogeo}$ by setting a very low refractive index contrast between the buffer and the guiding layers for a given geometry, planar for instance. It is accessible thanks to our previous studies showing that the refractive index contrast can be tuned by controlling the composition of the above mentioned ORMOSIL material and can be as low as 2 x 10^{-3}[32].
The second strategy to reduce $LB_{optogeo}$ relies on the fabrication of waveguides structures of specific shape to access very low $LB_{optogeo}$ for a given refractive index contast.
To combine these two strategies, We chose rib waveguides since an additional geometry parameter can be tunded to minimize the $LB_{optogeo}$ [18, 24] in comparaison with the planar chirowaveguides . Figure 2-c (inset) is cross-sectional schematic of the targeted rib waveguide. It is characterized by a strip width (w), a strip height (h), and a slab thickness (d). The guiding and the buffer layers have refractive indices n_1 and n_2 respectively ($n_1 > n_2$). The structure is studied in air (refractive index of cover layer n_0=1). Gathering those specifications, we have computed the guided modes properties via a full vectorial mode solver for different rib sizes and refractive index contrast limited to waveguides with two first fundamental polarization modes[33]. Figure 2-c) shows the computed $LB_{optogeo}$ as a function of strip width w at constant d=0.2 µm and h=2.1 µm having refractive index contrast n_1-n_2=15 x 10^{-3} (red line) and n_1-n_2=15 x 10^{-2} (blue line). The colored area delimit the w ranges where $LB_{optogeo} \leq CB$ which corresponds to the targeted ellipticity angle $\chi > \pi/8$. Comparison of the red and blue curves shows that the higher the refractive index contrast, the narrower the zone where $LB_{optogeo} \leq CB$. Quantitatively, it corresponds to $w = 3.20\mu m \pm 80$ nm and $w = 2.7\mu m \pm 40$ nm for the low and high refractive index contrast respectively. Consequently,the lower the refractive index contrast, the lower the constrain on w. This illustrates the importance to optimize both the refractive index contrast and the geometry of the guiding layer at the same time.
While $LB_{optogeo}$ is possible to compute and technologically tunable, LB_{stress} is difficult to predict and to control practically[22]. Our strategy to get rid of this unpredictable LB_{stress}, has been to elaborate different rib waveguides with a constant d and h but with a series of w values, $0.3\mu m$ step-wise around the computed zero optogeometric birefringence, on the same chip. Thus, by getting positive and negative $LB_{optogeo}$ the stress linear birefringence should be cancelled.

2 Rib fabrication and testing

Among the different methods to obtain structured materials of high optical quality, the combination of sol-gel based methods and imprint lithography is efficient [34, 35, 36]. Thus, we also have used this combination to realize the rib waveguides made of ORMOSIL, for this study.

Material Synthesis: Using the approach previously published by our group[37], we synthesized sols mainly based on a polymerizable triethoxysilane precursor functionnalized by a chiral binaphtol group called RSi(OEt)3. While the binaphtol is a molecule available as its two enantiomers, the use of (+)RSi(OEt)3 or (–)RSi(OEt)3 gives access to a material with opposite chirality. By mixing both (+)RSi(OEt)3 and (–)RSi(OEt)3 in equivalent proportions (50-50)% , racemic material is obtained for the fabrication of achiral channels as control samples. The refractive index and the quality of the final deposited layers have been adjusted by addition of controlled amount of pre-hydrolysed MTEOS and PEG200 to the sol. Varying the concentration in tetrahydrofuran and the dip coating withdrawal speed, the thickness of the deposited layers can be controled.

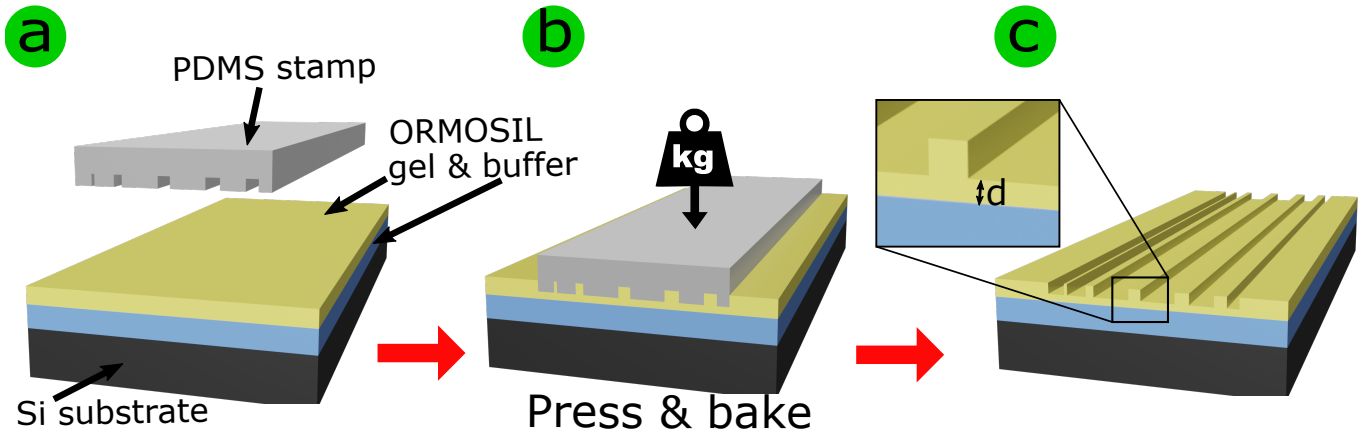

Figure 3: Schematic representation of the imprint lithography process flow. **a)** Deposition of a fresh ORMOSIL layer on a fully condensed buffer layer. **b)** Pressing the PDMS stamp into the ORMOSIL gel and baking them. **c)** Fabricated ORMOSIL structure after demolding of the stamp from the ORMOSIL

Structuring: Figure 3 presents the used process flow for the sample shaping. After the fabrication of a homemade silicon master mold and PDMS stamp (see Methods for details), the imprint lithography has been performed in three straightforward steps: (a) Dip coating of the material sol on a fully condensed thick buffer layer made from the same sol but with a lower refractive index on a silicon substrate (Figure 3-a); (b) Pressing the PDMS stamp on to the freshly dip coated layer then baking the whole system until complete condensation (Figure 3-b); (c) Removing the stamp from the layer to get a negative image of the stamps structures (Figure 3-c).

Structures characterization: The pattern was first inspected by optical and scanning electronic microscopies (SEM). The SEM images in Figure 4 a-b show that the initial silicon patterns (ribs of w=1.8, 2.1, 2.7,... 5.1 µm) are well transferred to the ORMOSIL layer. The fabricated ribs have sidewall angle $80° < \alpha < 90°$ with a slight difference ($\leq \pm 4°$) between the two sides of the channels (Figure 4-b) coming from different anisotropic imperfections during the fabrication process. The channels strip widths w and strip heights h are very similar to the initial master dimensions with a variation of $\pm 0.05 \mu$m from one waveguide to the other. According to SEM measurement, we clearly see that sidewall roughness are very low which was confirmed by the low losses measurement (SI Sec. 3). For a given rib, inspection with an optical microscope does not show any dimensions' variation along a 2 cm long chip. Moreover, polarization measurements performed on a 2 cm long waveguide before and after a half-cut do not show any differences. This ascertains that the cross-sectional shape of the waveguide does not vary significantly on the chips.

Optical propagation: Samples are cleaved then fixed on our optical setup (Figure 5). Light is launched and guided into each channel independently, strip height h slab thickness d are constant while w vary between 2.1 and 4 µm.
Losses are measured by light scattering from the channels top surface. About 10% of the ribs do not transmit the guided light at all due to some punctual defects on the chips. For all the others, the whole propagation losses are always below 3dB/cm, they become even lower after the first few millimeters of propagation that is attributed to the mode adaption between the input light and the guided mode (SI Sec. 3). After those first millimeters, the losses are difficult to detect, and they are estimated to be lower than 0.5 dB/cm.
Waveguides supporting only the two fundamental modes TE_{00} and TM_{00} were obtained for rib's widths lower than (3-3.3μm). The modes measured at the waveguide output are properly confined in the structure (Figure 4-c)) and with an intensity profile similar to the simulated one's (Figure 4-d)). The size of the guided mode image shown in Figure 4-c) reveal that the process ends up with a slab thickness of d

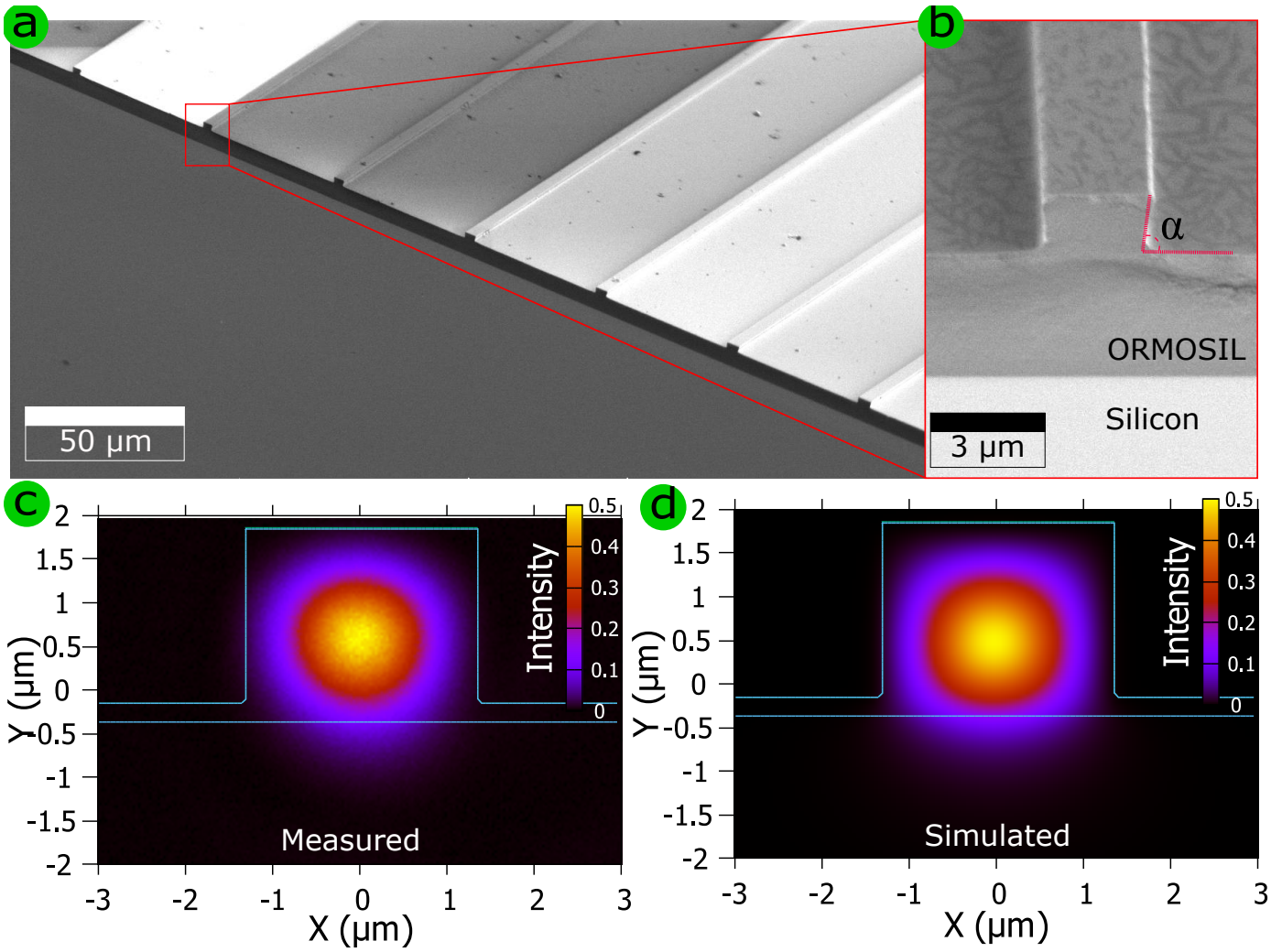

Figure 4: **a)** SEM image of the fabricated rib waveguides with different width. **b)** Fabricated rib with strip width (w=2.7µm) and strip height (h=2.1µ)m slab thickness (d=0.2µm). The buffer layer is 6µm thick with a refractive index difference Δn=0.015 with the rib region. The substrate is Si wafer. **c)** Measured and **d)** Simulated mode intensity profile for 2.1x2.7µm^2 rib.

=(0.2±0.01) μm.

3 Polarization results

All the results presented here were obtained by keeping background relative humidity at 57±2% while we have observed that a variation of 10% in the relative humidity results in a variation of ellipticity χ of about 0.05π for the waveguides with the highest eigenmode ellipticity. The channels have been studied using the setup shown in Figure 5: a 633nm laser beam passes through a polarization modulator, then is launched into the rib waveguides. The waveguides output light is characterized in terms of the Stokes parameters by using standard Stokes polarimetry[38]. Both the input and output light's state of polarization (SOP) are plotted on the PS in order to determine the effect of the waveguides on the polarization modes. For all waveguides with first two fundamental modes, the PS representation of the input/output SOP shows that all the waveguides are birefringent devices with unique eigen-axis depending on their CB and LB. We compare here the results of the waveguides made of the material with positive chirality (CB=+1 x 10^{-5}), negative chirality (CB=–1 x 10^{-5}), and racemic (CB=0) as a function of the channels' geometries.

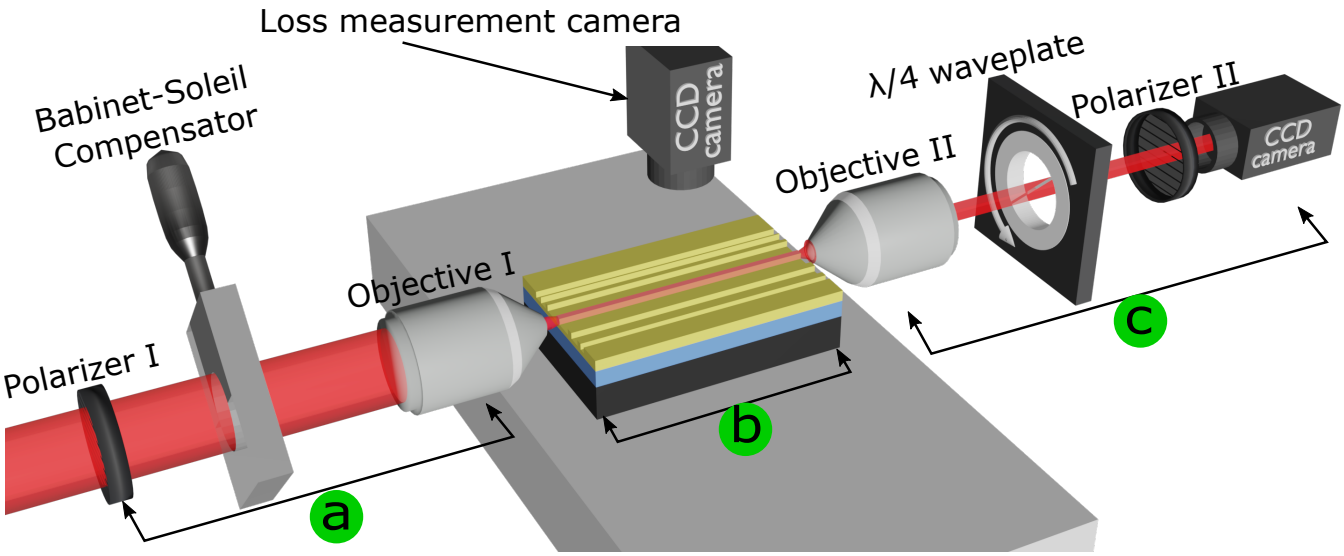

Figure 5: Optical measurement setup. **a)** The polarization of a laser beam is controlled by a combination of a linear polarizer and a Babinet–Soleil compensator then coupled to the sample with an optical objective. **b)** The guided light interacts with the sample (chirowaveguide). **c)** The propagated light is decoupled from the sample using another optical objective then its polarization state is analysed using combination of a rotating quarter waveplate and a linear polarizer.

Elliptical birefringence modulation: First, we investigate the effect of the strip width w on the polarization behavior of the waveguide. Figure 6 reports the measured eigenmodes ellipticities versus the strip width w on three chips with different chirality (+), (–) and racemic (+/–). Measurements are repeated on at least five successive series for each of the chips, resulting in error bars that are twice the standard deviation of the measurements. For a given dimension, we retain only the best 70% of the ribs. The 30% remaining ribs present lower eigenmodes ellipticity that comes either from uncertainty in the process width or from additional deformations contributing to a higher LB. Consistently with the position of their eigen-axis in the equatorial plane, the eigenmodes ellipticities of the racemic waveguides (black squares) are always null, behaving like achiral IP waveguides which are linear birefringent. Adding chirality to these waveguides profoundly change their behavior. For the same rib structure, from w=3.9µm down to $w = w_0 = 2.7$µm, the eigenmodes ellipticity increases from conventionnal TE/TM modes ($\chi = 0$) to nearly circularly polarized modes ($\chi = (0.18\pm0.04)\pi$ and $(-0.16\pm0.02)\pi$). Lowering the strip width from this optimized value results in a high reduction of the eigenmodes ellipticity down to 0.10π at 2.1µm.

Optimized LB: Three examples of PS input/output trajectories for the three (+),(–) and (+/–) chirality type are displayed in Figure 7, for the strip width w_0. These trajectories show the elliptical birefringence nature of the chirowaveguides with a clear rotation of the polarizations state around an eigen-axis out of the equatorial plane, while this rotation axis lies in the equatorial plane for the racemic samples attesting for an achiral LB device. Additionally, the input polarizations states are rotating "to the west" for the sample (+) which corresponds to a clock-wise rotation in the laboratory space and with the location of the slow eigenmode in the south hemisphere as expected for a (+)-enantiomer in a chiral medium. The sample (–) presents an opposite effect (mirror image) as expected for two enantiomers. Combining the measured eigenmode ellipticity and the rotation angle in the PS, we calculated via Eq. 4-Eq. 5 the two birefringences at this strip width w_0, we have obtained CB=(1±0.1) x 10^{-5} and LB=(4.5±1) x 10^{-6}. This CB value is very close to the CB measured on thick planar chiral films [32] and confirms the validity of the coupled mode approach.

Discussion – sources of LB: Our results show that by varying one geometrical parameter of the channel waveguides (the strip width w), the eigenmodes ellipticity can be tailored from 0 to $(0.18 \pm 0.04)\pi$, the maximum expected value being 0.25π. Indeed, as expected by the numerical computations shown

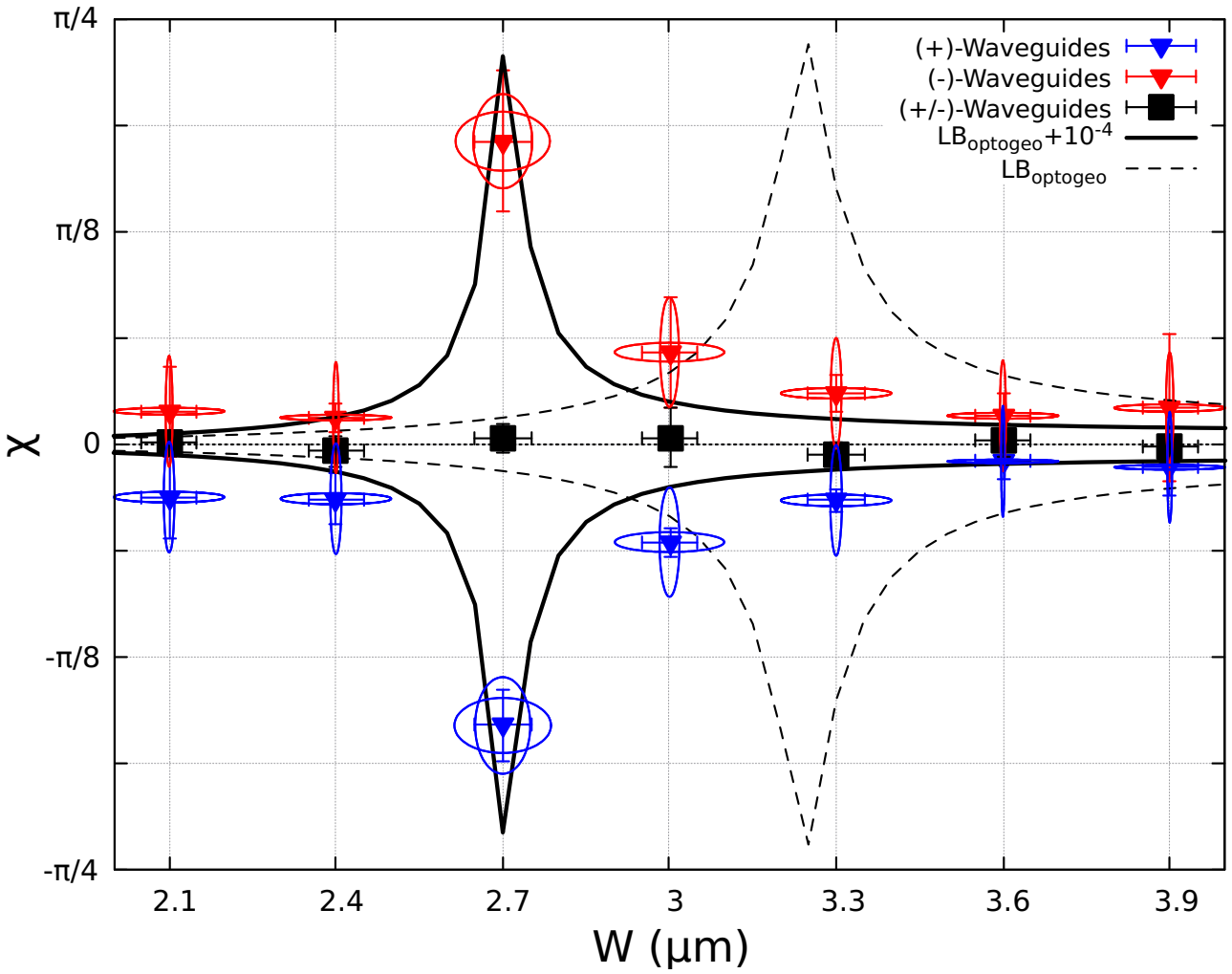

Figure 6: Eigenmodes ellipticity and polarization ellipses measured for different rib strip widths w at rib height h=2.1 μm, slab thickness d=0.2 μm, refractive index contrast n_1-n_2=0.015, and working wavelength is 630 nm. The black curves are the plot of the coupled mode theory ($\pm$arctan(|CB/LB|), Eq. 4) taking CB=$\pm$1 x 10^{-5} and computed $LB_{optogeo}$ (dashed line) and $LB_{optogeo}$ plus a constant LB = 1 x 10^{-4} (continuous line).

in (Figures 2-c), the values of $LB_{optogeo}$ is modulated with the w and should become almost zero at certain values of w. However, the highest measured eigenmode ellipticty is obtained at w=2.7 µm which is different from the expected value by the modeling: the measured value of w shifted by +0.5 µm from the calculated one (dashed line curve in Figure 6). If now, an additional (constant) contribution to LB (LB_{total}=$LB_{optogeo}$ + 1 x 10^{-4}) is used, the model perfectly fits the experimental data (continuous line curve Figure 6). Such additional constant linear birefringence contribution has been already observed for planar layer of polymers [39, 40] and is attributed to the non-matching thermal and mechanical properties of the different layers constituting the devices. Similarly, our fabrication procedure implies several layers of materials and can also add a constant stress because of the pressure applied during the imprinting. Thus, thanks to this modeling, the linear birefringence residual contributions (other than $LB_{optogeo}$) can be deeper investigated by analyzing the elliptical birefringence of the waveguides. Indeed, the eigenmode ellipticity determination allows to accurately measure LB using Eq. 4 (CB=1 x 10^{-5}) and to find the linear birefringence main axes.

We have plotted in Figure 8, the waveguides linear birefringence orientation and value versus w. For all the strip widths, LB value is lower than 1 x 10^{-4} and it is minimum at $w = 2.7$ μm where values as small as 3 x 10^{-6} are measured (Figure 8 bottom panel). Taking the total linear birefringence as LB_{total} = $LB_{optogeo}$ + LB_{stress} is enough to reproduce the experimental results of the LB with a sharp minimization of the values at $w = w_0$. Regarding the linear birefringence orientations (Figure 8 top panel), ex-

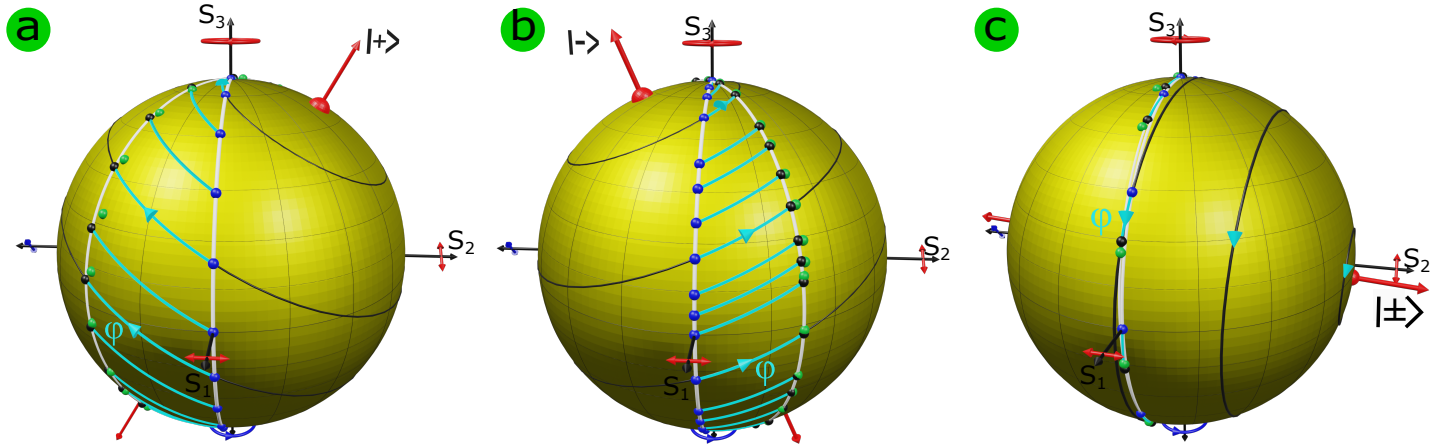

Figure 7: Poincaré representation of experimental results of input polarizations (blue points) and output polarization (green points) after propagation in a **a** (+) enantiomer, **b)** (–) enantiomer and **c)** (+/–) racemic rib waveguide of strip width 2.7μm. Interaction with the waveguides induces a φ rotation (light blue arrows), which converts the input polarization to the output polarization states (black points). The rotation axis (red arrows) defined the waveguide's eigen-polarization states.

cept for $w = w_0$, they are all around zero whatever the waveguides width and thereby respect the planar geometry of the chips. At $w = w_0$, unexpectedly, the linear birefringence orientation don't belong anymore to the plan of the device as deduced from the LB orientation values (Figure 8 top panel). Analogously, Figure 7 illustrates results for w_0 channels and demonstrates that the polarization ellipses are not aligned to the "horizontal/vertical" axes. As this behaviour is also observed for the racemic rib waveguides, with an eigen-axis oriented along the $\psi = \pm 0.25\pi$ on the PS (Figure 7-c), it can not be attributed to chiral effect. Around w_0, the LB orientation tells that when $LB_{total} \leq 1 \times 10^{-6}$, another source of linear birefringence arises not following the chip geometry. It probably images the small departure from the ideal TE/TM rectangular symmetrical shape and can be attributed to the slight sidewall angle α difference ($\pm 4°$) observed on some of the ribs as can be seen on the SEM images (Figure 4-b). This "disymmetry" birefringence ($LB_{disymmetry}$) can only be observed when the $LB_{optogeo}$ is low enough to be canceled by the LB_{stress}. It affects the eigenmodes axis orientation but it does not impact the eigenmodes ellipticity as its small value keeps LB_{total} smaller than CB.
Finally, the linear birefringence of the studied ribs can be assigned to three sources: (i) the variable opto-geometrical birefringence $LB_{optogeo}$ (for ideal rectangular symmetrical shape), depending here on w, (ii) a constant stress birefringence $LB_{stress}=1 \times 10^{-4}$, and (iii) a low birefringence $LB_{disymmetry} \leq 1 \times 10^{-6}$ not following the chip geometry and only observable when the two precedent LB cancel each other. This analysis demonstrates the relevance of our design strategy to produce low LB waveguides by scanning the opto-geometrical birefringence $LB_{optogeo}$ over a wide range of channel width. Indeed, it made it possible to compensate the uncontrolled linear birefringence $LB_{stress}=1 \times 10^{-4}$ arising in our devices. However a remaining birefringence contribution, extremely low ($\sim 1 \times 10^{-6}$), can not be compensated because it doesn't have the same orientation as the other contributions. This non TE/TM oriented birefringence sets the ellipticity limit of our devices to $\chi = (0.18 \pm 0.04)\pi$.

Conclusion and outlook

We have achieved optical rib waveguides with non-conventional elliptical eigenmodes. Using a chiral material with high CB, we designed and imprinted rib waveguides with a linear birefringence around the material's circular birefringence. The description of chirowaveguides as conventional TE/TM devices perturbed by chirality put forward CB and LB as the only two parameters ruling the polarization properties of the eigen modes propagating in these systems. Thus, for a certain CB value, intrinsic to the chiral material and by screening the waveguide optimal geometry, using a simple PDMS imprint pro-

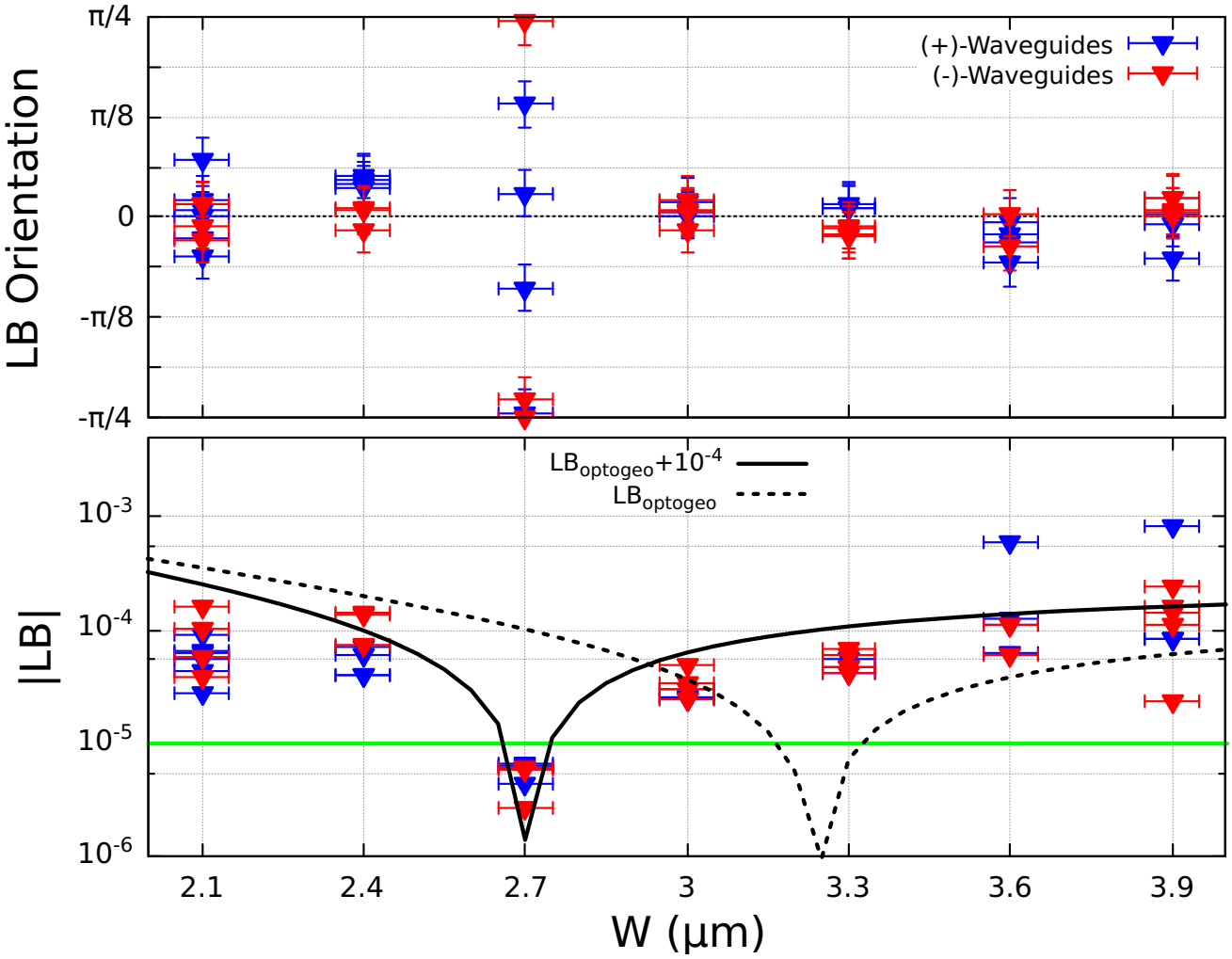

Figure 8: Experimental linear birefringece LB. Top: axes orientation of the eigen-polarization ellipse, Bottom: intensity. The black curves are the plot of the form birefringence (dashed line) and the sum of the form birefringence and a constant birefringence of 10^{-4} (continuous line).

cess, we were able to elaborate optical channel chirowaveguides with a tunable LB. Moreover, elliptical birefringent rib waveguides with tailored ellipticity angle χ from 0 to 0.18π are realized on the same chip in only one imprint process. Consequently, the polarization of eigenmodes propagating in these systems, without modiffication, could be tuned from linear to quasi-circular. These results pave the way for the next generation of IP circuits with components of different birefringences on the same chip. For instance, the combination of a chiral waveguide with an achiral one could convert the TE polarization to any other polarization by rotation on two axes in the Poincaré sphere. Moreover, by allowing the propagation of eigenmodes with polarizations other than the famous TE/TM, the practical realization of these chirowaveguides significantly expand the scope of IP circuits and enable the development of new polarization-related devices. The light being a chiral probe, through its circular polarizations, one potential application of these channel chirowaveguides could be on-chip chiroptical sensors.

Acknowledgement

Authors acknowledge support from Agence Nationale de la Recherche (project CAPTOR ANR-18-CE06-0010).

Experimental section

Silicon master and PDMS stamp fabrication Figure SI-3 schematically presents the complete fabrication process. Photoresist channel structures with targeted size are made on a silicon wafer (Figure SI-1). These structures are etched into the substrate in a reactive ion etching process using mixture of SF_6 and O_2 gases. The remaining photoresist is then lift off in an ultrasonic wetbench to have pure silicon structures. In this step, channels with same height but different width are obtained on a silicon wafer. The surface of the cleaned mold is then functionalized with a fluorosilane (Trichloro(1H,1H,2H,2H-perfluorooctyl) silane) by vapor phase deposition in a desiccator (under vacuum) for 3 h. This creates an anti-sticking layer on the mold to improve demolding during PDMS replication. The silicon structures are then replicated by casting liquid Polydimethylsiloxane (PDMS) against the mold. After baking the ensemble (PDMS on silicon) at 70 °C for 3 h and peeling off, negative image of the mold is transferred into a cross-linked flexible PDMS stamp.

Buffer layer preparation Prior to ORMOSIL buffer layer deposition, silicon substrates are cleaned in a freshly prepared piranha solution (Figure SI-2). Thick ORMOSIL buffer layers are dip coated on the clean silicon substrates. These buffer layers are annealed at 120 °C for 20 h to get complete condensation of the films.

Optical setup The setup is schematically presented in Figure 5. A laser beam at 630nm is coupled into the rib waveguide through a microscope objective as the input. The beam polarization is modulated by a Babinet-Soleil compensator to produce any polarization ellipses with main axes horizontal/vertical. After guiding the light in the rib waveguide, it is collected by another microscope objective, then send through a polarization analyser (rotating quaterwaveplate plus analyzer) and subsequently imaged on a CCD camera. Analysing the image intensity versus the quarterwaveplate rotation angle allows to extract the Stokes parameters of the output light[38]. The propagation losses were measured from the decay of light scattered out of the waveguides and recorded with a camera imaging the top of the channels.

References

[1] A. Yariv and P. Yeh. *Optical waves in crystals*. Wiley New york, 1984.

[2] B. E. A. Saleh and M.C. Teich. *Fundamentals of Photonics*. John Wiley and Sons, 2007.

[3] D. L. Andrews. Quantum formulation for nanoscale optical and material chirality: symmetry issues, space and time parity, and observables. *Journal of Optics*, 20(3):033003, February 2018.

[4] Stewart E Miller. Integrated optics: An introduction. *The Bell System Technical Journal*, 48(7):2059–2069, 1969.

[5] Enrique AJ Marcatili. Dielectric rectangular waveguide and directional coupler for integrated optics. *Bell System Technical Journal*, 48(7):2071–2102, 1969.

[6] L. D. Barron. Symmetry and molecular chirality. *Chem. Soc. Rev.*, 15:189–223, 1986.

[7] H. Poincaré, M. Lamotte, and D. Hurmuzescu. *Théorie mathématique de la lumière*. Cours de la Faculté des Sciences de Paris. Cours de physique mathématique. Georges Carré.

[8] P. Pelet and N. Engheta. The theory of chirowaveguides. *IEE Transactions on Antennas and Propagation*, 38(1):90–98, January 1990.

[9] M Oksanen, P.K. Koivisto, and I.V. Lindell. Dispersion curves and fields for a chiral slab waveguide. *IEE Proc., Part H: Microwaves, Opt. Antennas*, 138(4):327–334, Aug 1991.

[10] W.N. Herman. Polarization eccentricity of the transverse field for modes in chiral core planar waveguides. *J. Opt. Soc. Am. A*, 18(11):2806–18, 2001.

[11] Jianguo Xiao, Keqian Zhang, and Lian Gong. Field analysis of a general chiral planar waveguide. *International Journal of Infrared and Millimeter Waves*, 18(4):939–948, 1997.

[12] Shinzo Muto, Tomoyasu Sakagami, Yoshihiko Sakane, Akira Namazue, Eisuke Nihei, and Yasuhiro Koike. TE-TM mode converter using optically active polymer. *Optical Review*, 3(2):120–123, mar 1996.

[13] W.N. Herman, Y. Kim, W. L. Cao, J. Goldhar, C. H. Lee, M. M. Green, V. Jain, and M.-J. Lee. Amorphos thin films of chiral binaphtyls for photonic waveguides. *J. Macromol. Sci., Part A: Pure Appl. Chem.*, 40(12):1369–1382, 2003.

[14] Stéphan Guy, Bruno Baguenard, Amina Bensalah-Ledoux, Dalila Hadiouche, and Laure Guy. Full polarization control of optical planar waveguides with chiral material. *ACS Photonics*, 4(11):2916–2922, 2017.

[15] Akihiro Tagaya and Yasuhiro Koike. Compensation and control of the birefringence of polymers for photonics. *Polymer Journal*, 44(4):306–314, April 2012.

[16] R Wolfe, VJ Fratello, and M McGlashan-Powell. Thin-film garnet materials with zero linear birefringence for magneto-optic waveguide devices. *Journal of Applied Physics*, 63(8):3099–3103, 1988.

[17] N Sugimoto, Y Katoh, and A Tate. Magneto-optic buried channel waveguides for a 45° nonreciprocal waveguide rotator. *Applied physics letters*, 63(20):2744–2746, 1993.

[18] K.S. Chiang and W.P. Wong. Rib waveguides with degenerate polarised modes. *Electronics Letters*, 32:1098, 1996.

[19] Wa Peng Wong and Kin Seng Chiang. Design of optical strip-loaded waveguides with zero modal birefringence. *Journal of lightwave technology*, 16(7):1240–1248, 1998.

[20] SY Cheng, KS Chiang, and HP Chan. Birefringence characteristics of benzocyclobutene rib optical waveguides. *Electronics Letters*, 40(6):372–374, 2004.

[21] J Enrique Vázquez-Lozano and Alejandro Martínez. Toward chiral sensing and spectroscopy enabled by all-dielectric integrated photonic waveguides. *Laser & Photonics Reviews*, 14(9):1900422, 2020.

[22] Md. Faruque Hossain, Hau Ping Chan, and Abbas Z. Kouzani. Efficient design of polarization insensitive polymer optical waveguide devices considering stress-induced effects. *Opt. Express*, 22(8):9334–9343, Apr 2014.

[23] H Dammann, E Pross, G Rabe, W Tolksdorf, and M Zinke. Phase matching in symmetrical single-mode magneto-optic waveguides by application of stress. *Applied physics letters*, 49(26):1755–1757, 1986.

[24] M. Lohmeyer, N. Bahlmann, O. Zhuromskyy, H. Dotsch, and P. Hertel. Phase-matched rectangular magnetooptic waveguides for applications in integrated optics isolators: numerical assessment. *Opt. Com.*, 158(1):189–200, 1998.

[25] D Keller, C Bustamante, M F Maestre, and I Tinoco. Imaging of optically active biological structures by use of circularly polarized light. *Proceedings of the National Academy of Sciences*, 82(2):401–405, 1985.

[26] Xiuli Yin, Jingjing Ding, Song Zhang, and Jilie Kong. Enantioselective sensing of chiral amino acids by potentiometric sensors based on optical active polyaniline films. *Biosensors and Bioelectronics*, 21(11):2184–2187, 2006.

[27] Dominik Niemietz, Pau Farrera, Stefan Langenfeld, and Gerhard Rempe. Nondestructive detection of photonic qubits. *Nature*, 591(7851):570–574, March 2021.

[28] Amnon Yariv and James F. Lotspeich. Coupled-mode analysis of light propagation in optically active crystals. *J. Opt. Soc. Am., JOSA*, 72(2):273–277, Feb 1982.

[29] P. Pelet and N. Engheta. Coupled-mode theory for chirowaveguides. *J. Appl. Phys.*, 67(6):2742–5, 1990.

[30] S. Huard. *Polarization of light*. Wiley, 1997.

[31] Dennis H. Goldstein. *Polarized Light*. CRC Press, Boca Raton, FL, USA, 2017.

[32] D. Hadiouche, C. Le Luyer, L. Guy, A. Bensalah-Ledoux, S. Saoudi, H. Khireddine, and S. Guy. Optimization of optical properties of high chiral planar waveguides obtained from a non-aqueous sol gel method. *Optical Materials*, 36(5):885–891, March 2014.

[33] L. Bolla. Empy [computer software]. 2017.

[34] C Jeffrey Brinker and George W Scherer. *Sol-gel science: the physics and chemistry of sol-gel processing*. Academic press, 2013.

[35] Stephen Y Chou, Peter R Krauss, and Preston J Renstrom. Imprint lithography with 25-nanometer resolution. *Science*, 272(5258):85–87, 1996.

[36] Younan Xia and George M Whitesides. Soft lithography. *Annual review of materials science*, 28(1):153–184, 1998.

[37] L. Guy, T. Vautey, and S. Guy. The use of LCMS as an analytical tool for hydrolysis/polycondensation monitoring of a chiral ormosil precursor. *J. Sol-Gel Sci. Technol.*, 52:146–152, 2009.

[38] H. G. Berry, G. Gabrielse, and A. E. Livingston. Measurement of the stokes parameters of light. *Applied Optics*, 16(12):3200–3205, 1977.

[39] Shashikant G. Hegde and Suresh K. Sitaraman. Stress-induced birefringence in siloxane polymer waveguides. *Applied Physics Letters*, 91(8):081114, 2007.

[40] A. Kilian, J. Kirchof, G. Przyrembel, and W. Wischmann. Birefringence free planar optical waveguide made by flame hydrolysis deposition (FHD) through tailoring of the overcladding. *Journal of Lightwave Technology*, 18(2):193–198, feb 2000.